CHAOTIC BEHAVIOUR OF A MEMBRANE RESONATOR WITH NANOWIRE ARRAY

Yuerui Lu, Manoj Pandey, and Amit Lal*
*Sonic*MEMS Laboratory, School of Electrical and Computer Engineering
Cornell University, Ithaca, NY, USA

ABSTRACT

We report the first chaotic behavior of a membrane mechanical resonator with a nanowire (NW) array structured surface. Compared with the control sample without NW array, the membrane resonator with NW array structured surface, can easily transition from linear operation to a nonlinear motion at resonance, and further to a chaotic state, through an increase in its dynamic operating amplitude. The high nonlinearity of the device spreads the concentrated excitation energy from a single frequency to a broad-band frequency range, which could be useful for line-spectrum vibration isolation. We develop a set of possible reasons for the chaotic behavior, which aid in future investigation of controlled chaotic structures.

INTRODUCTION

Nano-scale resonance systems can transition from a linear resonance operation to a nonlinear one through an increase in its dynamic operating amplitude. In the nonlinear regime of nano-electro-mechanical system (NEMS), phenomena, such as hysteresis [1], spring hardening [2], and pull-in [3], can occur. The nonlinear dynamical properties of the NEMS have been exploited for many applications. For instance, noise-enabled transitions in a nonlinear resonator were analyzed to improve the precision in measuring the linear resonance frequency [4], and a homodyne measurement scheme for a nonlinear resonator was proposed for increasing the mass sensitivity and reducing the response time [5].

The nonlinear dynamics of NEMS system might lead to the appearance of chaos. Chaotic behavior of a dynamical system is highly sensitive to initial conditions. Chaos can be observed in many natural systems, such as weather, where infinitesimally small perturbations can cause large effects. For chaotic systems, small differences in initial conditions will result in widely diverging outcomes, leading to system outcome prediction impossible [6]. Normally, such behavior may be investigated or explained through analysis of a chaotic mathematical model, or through analytical techniques such as recurrence plots and Poincaré maps. Nonlinearity, especially chaos, in NEMS systems has mostly been seen as a problem, but here we might want to ask whether one can explore chaos to enhance its applicability.

Here, we report the first chaotic behavior of a membrane mechanical resonator with nanowire (NW) array structured surface. Compared with the control sample without NW array, the membrane resonator with NW array structured surface (Fig.1), can easily transit from linear resonance operation to a nonlinear one, and further to a chaotic state, through an increase in its dynamic operating amplitude. The high nonlinearity of our device will help to spread the concentrated excitation energy from line-spectrum frequency to a broad-band frequency range (Fig.2 & 3), which could be used for line-spectrum vibration isolation [7]. Vibration isolation is needed for MEMS device [8]; for example, inertial sensors, especially MEMS gyroscopes, can be interfered or even damaged by the undesired modes of vibration present in mechanically harsh environments. For a linear vibration isolation system, frequency conservation is the main characteristics. For nonlinear oscillations, external harmonic excitation from noise can exhibit a great variety of harmonic responses, sometimes countless when chaos appears The concentrated energy therefore spreads from the frequency of excitation to a broad-band frequency range (Fig.2). For the given input energy, the response energy at the excitation frequency for the chaotic vibration system is much less than that for the linear vibration system [7]. Hence, a chaotic energy dissipater could be used to isolate sensors from external vibrations.

DEVICE FABRICATION

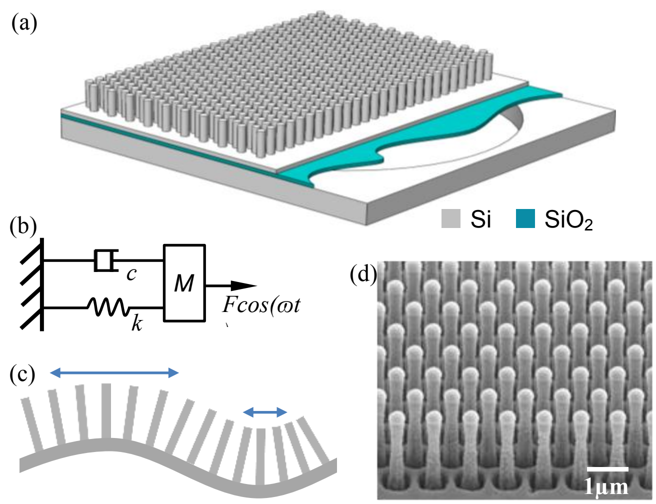

Figure 1: (a) Schematic for device structure. Vertical Si nanowire (NW) array were patterned on Si/SiO_2 (1 µm/2 µm in thickness) bilayer circular membrane (diameter 800 µm).(b) Schematic for the single degree of freedom model with damping. (c) Schematic for the space modulation of the NWs by the standing wave of the membrane. (d) SEM image of the NW array.

For device fabrication, we used electron beam lithography to pattern the vertical silicon NW arrays, on a SOI wafer, by silicon reactive ion etching (RIE) using SiO_2 nano-posts as the etching mask. The vertical silicon NW array has 300 nm of wire diameter, 1 µm of pitch and 3.5 µm of height (Fig.1b). These NW arrays show uniform wire diameter, controllable wire orientation and wire pitch spacing. Optical lithography with backside alignment was used to pattern the backside circular cavity (800 µm diameter), followed by a silicon DRIE to etch through the silicon substrate using the SOI buried oxide as the stopping layer. A PZT plate was adhesively bonded to the silicon backside to actuate the membrane.

EXPERIMENTAL OBSERVATIONS

The vibration response of the membrane was measured by an optical interferometer (PolyTec^{TM}). Power-spectrum density characteristics (Fig.2) of the devices were measured by using a power spectrometer to analyze the output signal from the interferometer. The *vibration amplitude* versus *time* was measured using an oscilloscope and a spectrum analyzer. For the membrane with NWs, we observed the fundamental resonance mode (f_1) at 163 kHz. When the system operates in linear range with low driving voltage 20 mV, the output signal shows monotonic spectrum (Fig.

2a top). The device can easily transition from linear resonance operation to nonlinear one, by increasing the PZT driving voltage. Initially, super harmonic nonlinear modes, such as $2f_1$ and $3f_1$, showed up at higher driving voltage (100 mV). Since the samples with and without NW are on the same chip and share the same PZT for actuation, the coupling from the PZT was the very similar in two samples. In the non-membrane area, the amplitudes of the NW versus non-NW samples were in the ratio of around 1:3, since the sample without NW has higher Q value (Table 1). When we increased the driving voltage further, the resonance modes and super harmonic modes will start to split into symmetric sub-bands, through bifurcation process. Finally, chaotic behavior of the device was observed (Fig.2a bottom), at 300 mV driving voltage. In the chaotic state of the device, the concentrated excitation energy was spread from line-spectrum frequency to many peaks over broad frequency range. The measurement of upper frequency range was limited by the range of the spectrum analyzer. The nonlinearity

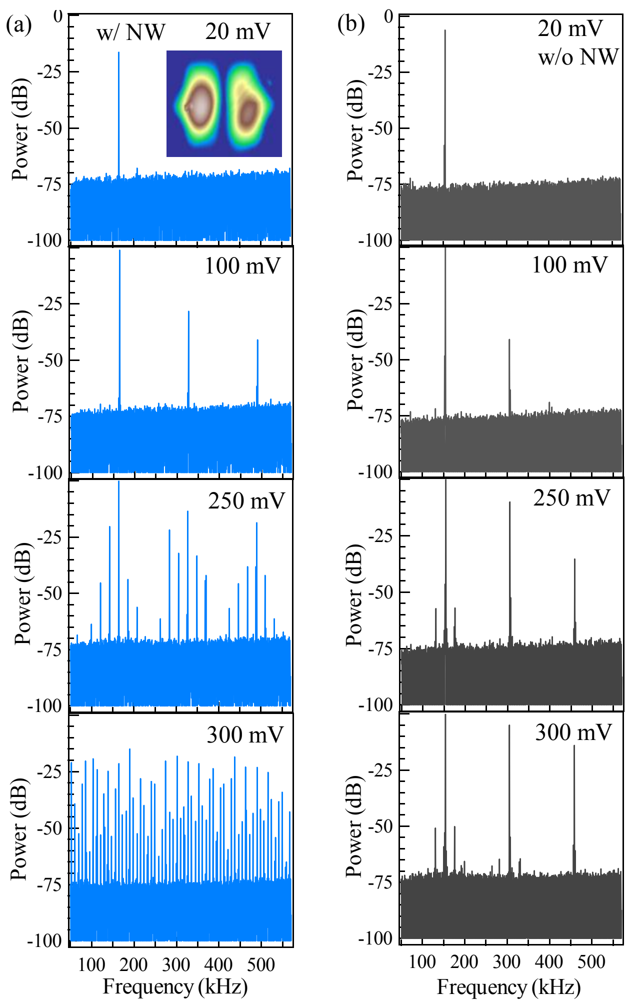

Figure 2: (a) Power-spectrum density characteristics of the membrane with NW at its resonant mode, when the device is driven by PZT under driving voltages of 20, 100, 250, 300 mV. Inset shows the measured standing wave vibration amplitude 2D mapping pattern of the mode 163 kHz. During mapping, the actuation frequency was fixed at the resonance mode and the interferometer laser gun was controlled by a stage controller for lateral movement with sub-0.5 µm lateral resolution. (b) power-spectrum density of the control membrane without NW, when it is driven at the same driving voltages correspondingly.

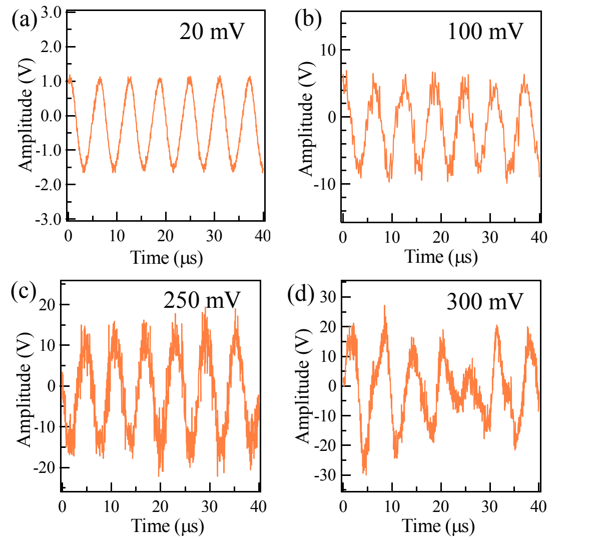

Figure 3: Output voltage vs. Time curves of the membrane with NW at its resonant mode, when the device is driven by PZT under driving voltages of 20, 100, 250, 300mV, for a-d, respectively.

originates from mechanical vibration and not optical detection nonlinearities as the maximum measured device vibration velocity was much less than the dynamic range of the interferometer used.

Moreover, we did the same measurement on the control sample, a Si membrane device without NW. The control sample was fabricated on the same chip, sharing the fabrication processes with the NW membrane device. These two samples have the same membrane size. For the control sample, a close resonance mode (f_2) at 153 kHz was observed, compared to the 163 kHz for the NW sample. The NW sample is lower frequency probably due to the lower effective density of the membrane. The power-spectrum density characteristics of this mode (Fig. 2b) ware also investigated as comparison. At higher driving voltage, super harmonic nonlinearity modes, such as $2f_2$ and $3f_2$, could be observed. However, compared with the membrane device with NWs, the control sample did not show obvious mode bifurcation process under the driving voltage. Even though much higher driving voltage was used and the device vibration velocity was reaching the upper dynamic limit of the interferometer, no chaos was observed on the control sample.

POTENTIAL SOURCES OF NONLINEARITY

The high nonlinearity of our NW array membrane resonator comes from several reasons. Firstly, the NW array structured surface introduces large surface roughness to the membrane on one side, leading to the broken of symmetry when the membrane vibrates. Secondly, the membrane has significant nonlinearity in tension version compression. Thirdly, air-damping will also introduce significant nonlinearity to the system. These NWs can enhance the total surface area by a factor of 10, leading to larger the air-damping force. In following section, we would like to focus on the modeling of nonlinearity from air-damping.

MODELING AND ANALYSIS

By considering damping, the nonlinear partial differential equation governing the membrane can be obtained as equation [9]:

$$\rho h \frac{\partial^2 Z}{\partial t^2} + D\nabla^4 Z + \zeta \frac{\partial Z}{\partial t} = f(r,\theta,t) \qquad (1)$$

where $Z(r,\theta,t)$ is the transverse displacement, ζ is the damping coefficient, h is the effective membrane thickness, ρ is the effective mass density, and D is the effective flexural rigidity of the membrane, and ∇^2 is the Laplacian.

By solving this equation for a circular membrane with radius r_0, the resonant frequencies and their corresponding transverse displacement profiles at different mode shapes are obtained as follows [10]:

$$f_{mn} = \frac{1}{2\pi}\sqrt{\frac{\gamma_{mn}^4 D}{\rho h}} \tag{2}$$

$$Z_{mn}(r,\theta) = \left[J_m(\gamma_{mn} r) - \frac{J_m(\gamma_{mn} r_0)}{I_m(\gamma_{mn} r_0)} I_m(\gamma_{mn} r) \right] \cdot [A_{1m}\sin(m\theta) + A_{2m}\cos(m\theta)] \tag{3}$$

where the functions $J_m(\gamma_{mn} r)$ and $I_m(\gamma_{mn} r)$ are the Bessel function and the modified Bessel function of the first kind, γ_{mn} are the eigenvalues and the subscripts m and n represent the number of nodal diameters and nodal circles for the vibration mode, respectively.

Symmetric circular discs under high-amplitude excitation have been shown to undergo bifurcation, leading to chaotic motion [11]. This happens due to the presence of cubic nonlinearity in the system, which becomes prominent at large amplitude vibrations, where energy is spread into different modes of the disc. The mode mixing results in the excitation of other energy modes, from what is being directly forced. This results in the quasi-periodic response of the directly excited mode which may become chaotic. It has also been shown that if structural symmetry in such systems is broken, the chaotic transition becomes possible at a much lower forcing [11]. Additionally the route to chaos is through period doubling, which is what is observed in the current system. Hence the presence of NW brings down the forcing threshold for the chaos, which can now be observed at relatively lower amplitude forcing. In order to handle the complexity of the analysis we obtain a reduced ordered set of equations for the system at hand by projecting the governing partial differential equation of the system motion, on to the dominant linear modes and hence obtain a set of ordinary differential equations, which are integrated using a 4th order Runge-Kutta based ODE solver. The governing equations used for the simulations are [12]:

$$\ddot{x} + \alpha\dot{x} + \gamma\dot{x}^2 - \omega_0^2 x + \beta x^3 = F\cos(\omega t) \tag{4}$$

where x is the position displacement, α is the linear damping coefficient, γ is the quadratic damping coefficient, ω_0 is the resonance frequency of the system, β is the Duffing's cubic nonlinearity coefficient, F is the external excitation force and ω is the frequency of the external force.

Previous theoretical reports [12] showed that damping force plays an important role in the nonlinear dynamics of a Duffing's oscillation system, which is also confirmed by our simulation results. We simulated the Poincare maps (Fig. 4) for two different cubic nonlinear systems with: 1) linear damping, and 2) quadratic damping. Poincare map for the system is obtained by plotting the solution at every forcing time period, which shows the periodic vibrations at the forcing frequency, with one point, while period doubling is shown with twice the number of points. Figure 4b shows that quadratic damping has lower forcing threshold value for the chaos, among these three systems. For the system without damping, we did not get chaotic behavior in the force range simulated, which indicates that it has the highest forcing threshold value for the chaos. Therefore, the addition of damping or quadratic damping term of same order significantly reduces the forcing threshold value for chaos.

From our experiments, we observed that the membrane device with NWs did show higher damping, compared with the membrane without NWs. We measured three resonance modes on each device (Table 1). The modes for the device with NWs showed much lower quality factor values (40~75) than that of the modes from the device without NWs (250~350). The enhanced air damping might be due to the enhanced total surface area, by a factor of 10, from these high aspect ratio NW structures. The squeeze film damping between the nanowires is also expected to increase the damping

Based on fluid dynamics theory [13, 14], the drag force on an object is generally dependent on its velocity, υ, and there exist two

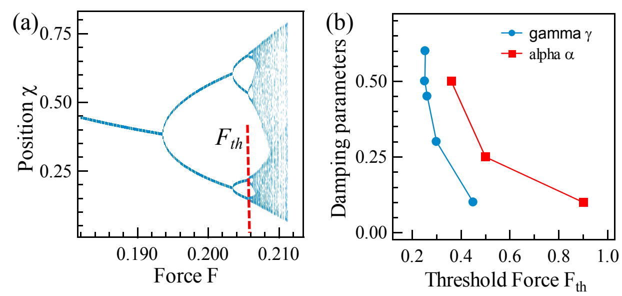

Figure 4: (a) Simulated Poincaré map of Position x vs. Force for a forced Duffing's oscillator with quadratic damping. Red dashed line indicates the threshold force (F_{th}) value for chaos. b) Simulated threshold force values as a function of the parameters for linear damping (alpha) and quadratic damping (gamma).

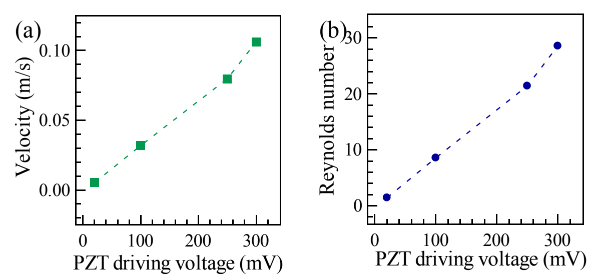

Figure 5: (a) Measured velocity as a function of the PZT driving voltage. (b) Calculated Reynolds number of our device based on the measured velocity and equation 5.

regimes where this dependence is either linear or quadratic. The parameter that differentiates these two regimes is the Reynolds number, R_e, which is the ratio of inertial to viscous forces,

$$R_e = \rho l \upsilon / \eta \tag{5}$$

where ρ is the fluid density, l is the characteristic cross-sectional length, υ is the velocity and η is the dynamic fluid viscosity. At high Reynolds number (R_e >10^3), drag is approximately dependent on the square of the velocity [14]:

$$f_d(\upsilon) = \frac{1}{2}\rho C_d A \upsilon^2 \tag{6}$$

where $f_d(\upsilon)$ is the velocity-dependent drag force where C_d is the drag coefficient, A is the cross-sectional area and. The drag coefficient, C_d, depends on the Reynolds number. At low Reynolds number (R_e <1), drag is linear with velocity [14]:

$$f_d(\upsilon) = 12\eta A\upsilon / l \quad (7)$$

Table 1: Comparison of the measured quality factor (in air) for the modes of the membrane sample with NW and without NW.

Membrane with NW		Membrane without NW	
f (kHz)	*Q*	*f* (kHz)	*Q*
163	42	153	337
107	38	101	265
234	73	218	352

Based on our measured velocity (Fig. 6a), the Reynolds number of our device is in the range of 1-50 (Fig. 6b). Therefore, the damping force for our system should be a combination of linear and quadratic damping. Moreover, based on equation 3 and 4, both linear and quadratic damping forces could be enhanced by the NW structure, due to the enhanced surface area.

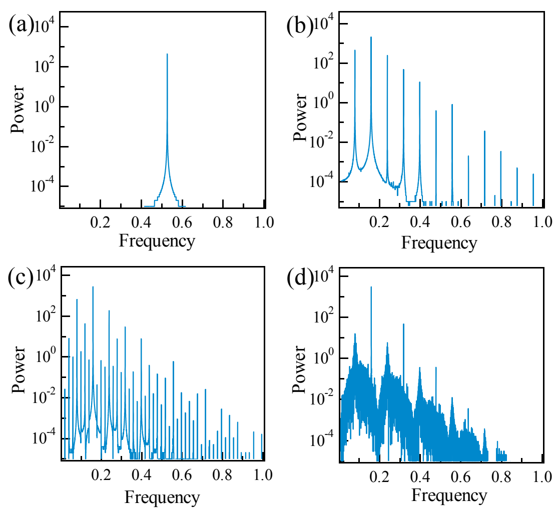

Figure 6: Simulated FFT of the motion at four different forcing levels: a) F=0.2 Single frequency responses, b) F=0.34 Multiple harmonics, c) F=0.206 Side-band bifurcation formation, d) F=0.38 Chaotic response.

Moreover, it has been previously shown [15] that in beam vibration problems, combination resonance can occur when the sum of the natural frequency of certain modes of the system is close to the sum of other modes of the system. In this case energy can transfer from higher modes of the system to the lower ones but no other way. Excitation close to the higher modes can lead to vibration of lower modes. This also leads to periodic modulation of primary mode being excited. However for this combination of the frequencies to be in an internal resonance, it is necessary that the governing equation have a quadratic nonlinearity term. This term seems to originate from the quadratic damping term that can be used to model the air drag. Here, the enhanced quadratic damping term from NWs might also trigger internal resonances, leading to lower threshold forcing value for chaos.

Of course, chaotic motion is a very complicated dynamic process, which is related to many factors [15]. In order to have a better understanding on the chaotic behavior of our device, more theoretical and experimental work is needed. Although hard to model, our system will be useful where energy dispersion is required. Also, our device provides a good platform to investigate nonlinearity dynamics and potential chaos engineering.

CONCLUSION

Chaotic behavior of a membrane mechanical resonator with NW array structured surface has been presented for the first time. Compared with the control sample without NW array, the membrane resonator with NW array structured surface, can easily transit from linear resonance operation to a nonlinear one, and further to a chaotic state, through an increase in its dynamic operating amplitude. The high nonlinearity of our device will help to spread the concentrated excitation energy from line-spectrum frequency to a broad frequency range. Our system will be useful where energy dispersion is required, such as for line-spectrum vibration isolation. Moreover, simulations on the dynamics of nonlinear systems with different damping have been investigated and possible reasons for the chaotic behavior are discussed.

REFERENCES

[1] I. Kozinsky, H. W. C. Postma, O. Kogan, A. Husain, M. L. Roukes, "Basins of Attraction of a Nonlinear Nanomechanical Resonator", Physical Review Letters 99, 207201 (2007).

[2] I. Kozinsky, H. W. C. Postma, I. Bargatin, M. L. Roukes, "Tuning nonlinearity, dynamic range, and frequency of nanomechanical resonators", Applied Physics Letters 88, 253101 (2006).

[3] S. N. Cha *et al.*, "Fabrication of a nanoelectromechanical switch using a suspended carbon nanotube", Applied Physics Letters 86, 083105 (2005).

[4] J. S. Aldridge, A. N. Cleland, "Noise-Enabled Precision Measurements of a Duffing Nanomechanical Resonator", Physical Review Letters 94, 156403 (2005).

[5] E. Buks, B. Yurke, "Mass detection with a nonlinear nanomechanical resonator", Physical Review E 74, 046619 (2006).

[6] S. H. Kellert, *In the Wake of Chaos: Unpredictable Order in Dynamical Systems*. University of Chicago Press. p. 32, 1993.

[7] J. Lou, *et al.* "Application of chaos method to line spectra reduction" Journal of Sound and Vibration. 286, 645 (2005).

[8] S. Yoon, *et al*. "Analysis and wafer-level design of a high-order silicon vibration isolator for resonating MEMS devices", J. Micromech. Microeng. 21, 015017 (2011).

[9] S. P. Timoshenko, S. Woinowsky-Kringer, *Theory of Plates and Shells* (New York: McGraw-Hill), 1959.

[10] M. Olfatnia, V. R. Singh, T. Xu, J. M. Miao, L. S. Ong, "Analysis of the vibration modes of piezoelectric circular microdiaphragms", *J. Micromech. Microeng,* Vol. 20, pp. 085013, 2010.

[11] C. Touze, O.Thomas, M.Amabili, "Transition to chaotic vibrations for harmonically forced perfect and imperfect circular plates", International Journal of Non-Linear Mechanics ,Vol. 46, Issue 1, pp. 234–246, (2011).

[12] A. Sharma, V. Patidar, G. Purohit, K.K. Sud, "Effects on the bifurcation and chaos in forced Duffing oscillator due to nonlinear damping", Communications in Nonlinear Science and Numerical Simulation, Vol.17, Iss.6, pp.2254-69, (2012).

[13] E. M. Purcell, *Am. J. Phys.* 453, (1977).

[14] J. P. Owen, W. S. Ryu, "The effects of linear and quadratic drag on falling spheres: an undergraduate laboratory", European Journal of Physics 26, 1085 (2005).

[15] C. Touzé, S. Bilbao, O. Cadot, "Transition scenario to turbulence in thin vibrating plates", Journal of Sound and Vibration 331, 412 (2012).

CONTACT

*Yuerui Lu, Email: yl676@cornell.edu